Latent heat method to detect melting and freezing of metals at megabar pressures

Zachary M. Geballe [1], Nicholas Holtgrewe,[1,2] Amol Karandikar,[1] Eran Greenberg [2], Vitali B. Prakapenka,[2]
and Alexander F. Goncharov[1]

[1]*Earth and Planets Laboratory, Carnegie Institution for Science, Washington DC 20015, USA*
[2]*Center for Advanced Radiation Sources, University of Chicago, Illinois 60637, USA*

The high-pressure melting curves of metals provide simple and useful tests for theories of melting, as well as important constraints for the modeling of planetary interiors. Here, we present an experimental technique that reveals the latent heat of fusion of a metal sample compressed inside a diamond anvil cell. The technique combines microsecond-timescale pulsed electrical heating with an internally heated diamond anvil cell. Further, we use the technique to measure the melting curve of platinum to the highest pressure measured to date. Melting temperature increases from ≈3000 K at 34 GPa to ≈4500 K at 107 GPa, thermodynamic conditions that are between the steep and shallow experimental melting curves reported previously. The melting curve is a linear function of compression over the 0–20 % range of compression studied here, allowing a good fit to the Kraut-Kennedy empirical model with fit parameter $C = 6.0$.

I. INTRODUCTION

High-pressure melting curves of simple materials provide a fertile testing ground for theories of melting, from simple empirical and semiempirical models such as the Kraut-Kennedy and Lindemann models [1,2], to atomistic models such as the *ab initio* Z method [3]. Knowledge of high-pressure melting temperatures is also crucial for understanding the evolution of planetary cores [4].

In order to test simple melting theories, accurate data are needed across a range of densities. In practice, compression up to tens of percent has been used [5]. To achieve this for the relatively incompressible transition metals, pressures of ≈ 50–100 GPa (0.5–1 megabar) are required. Recent publications have reported melting curves to pressures above 50 GPa for transition metals including V [6], Nb [7], Fe [8], Mo [9], Ti [10], Zr [11], Pt [12], and Ta [13]. Unfortunately, the accuracy of melting data is uncertain for several of the most-studied metals at pressures above 20 GPa, as evidenced by discrepancies among studies of Fe [8], Ta [13], Mo [9], and Pt [12]. For platinum, the experimental melting temperatures reported in Refs. [12,14] are systematically higher than those in Refs. [15–17], resulting in a discrepancy of at least 1000 K at 70 GPa, the pressure corresponding to 15% volume compression.

It may also be possible to test simple analytical models of melting by comparing them to *ab initio* models. For platinum, melting temperature calculations by two different research groups using the recently developed *ab initio* Z method agree to within 200 K at 10 GPa and within 300 K at 120 GPa [3,12]. The results imply an approximately linear dependence of melting temperature (T_m) with respect to pressure (P), but not with respect to volume (V), indicating a departure from the Kraut-Kennedy model if the error in calculated melting temperature is less than 400 K. Note that departures from

both the Lindemann and Kraut-Kennedy models are common (e.g., Refs. [18–20]), and the Lindemann model has been frequently criticized for its overly simplistic physical basis (e.g., Refs. [20,21]). Nevertheless, the accuracy of Z-method calculations is also uncertain, especially in the absence of waiting time analyses [22,23]. For platinum, the Z-method calculation results match the most recently published experimental data [12], but not others [15,16], underscoring the need for new experimental results, and perhaps new experimental methods that are more reproducible across laboratories than the methods currently used.

Commonly used melt criteria for diamond cell experiments include visual observation of motion, anomalies in temperature vs laser power, and the onset of diffuse scattering in x-ray diffraction. These three techniques account for all the experimental data on platinum melting at pressures above 20 GPa [12,14,14–17]. The first two criteria are indirectly related to melting. When materials melt, they tend to move and to cause anomalous temperature-power trends, but neither phenomenon is specific to melting, nor do they necessarily occur upon melting [10,11,24].

On the other hand, observation of a step-function increase in diffuse x-ray scattering upon increasing temperature would provide strong evidence for melting, because liquids generate much stronger diffuse scattering than crystalline solids. In reality, technical challenges related to large temperature gradients add substantial ambiguity to the identification of the onset of melting by x-ray scattering in laser-heated diamond anvil cells [25]. For the case of platinum, Anzellini *et al.* [12] reports precise x-ray-based determination of melting temperature up to 30 GPa, but not at higher pressure. The uncertainty in the temperature of liquid diffraction increases to ±700 K at 49 GPa, and no diffraction from a liquid is reported at higher pressures. The thesis of Lo Nigro [17] also reports a melting

curve from 30 to 90 GPa based on x-ray diffraction, but the platinum diffraction data is noisy in Fig. 3.5 of Lo Nigro [17], likely due to sample preparation methods designed to study the silicate sample in which a small amount of platinum is embedded. Few details are given about the melt criterion and measurement uncertainties, and the resulting melting curve is ~200 K to 1500 K lower than the plateau-based melting data of Anzellini *et al.* [12].

To identify melting in a more reproducible way than in previous experiments at pressures above 20 GPa, detecting latent heat could be very useful. All melting transitions have latent heat, and it is typically much larger than the latent heat of solid-solid transitions [26]. In practice, latent heat has been a useful way to identify melting of refractory metals at ambient pressure [27], but it has likely never been identified in static compression experiments at pressure >20 GPa. Albeit, in the case of pulsed-laser heating of hydrogen at 100–200 GPa, anomalies in peak temperature versus laser power have been attributed to the latent heat of melting and the latent heat of dissociation of molecular hydrogen [28–30]. Nevertheless, the attribution to latent heat is controversial [31,32], and the method of latent heat detection has not been reproduced by any other group, to the best of our knowledge.

The major experimental challenge in identifying latent heat in high-pressure experiments is to deposit heat and measure the sample's temperature (or a proxy for temperature) fast enough and over a large enough sample volume so that little heat is lost to the surroundings. Using finite element models, Geballe and Jeanloz [24] shows that the heating timescale should be ns to μs in order to reveal the latent heat. This timescale results from the inevitably small sample size and inevitably poor thermal insulation in diamond cell experiments. The models also show that latent heat signatures are larger during internal heating than surface heating, suggesting Joule heating of metals is preferable to laser heating of metals. So far, these extreme requirements have limited the detection of latent heat in static high-pressure experiments to the pressure range below 20 GPa and to devices with larger sample volumes than those in diamond anvil cells [18].

Here, we report a new technique that records melting by revealing the latent heat of melting of metals in diamond anvil cells at pressures in the range $\approx$7 GPa to above 100 GPa, and temperatures in the range $\approx$2200 K to above 4000 K. The technique integrates microsecond-timescale pulsed electrical heating with the internally heated diamond anvil cell for the first time, thereby creating the short heating timescale and spatial homogeneity needed to reveal latent heat at high pressures. We then use the technique to determine the melting curve of platinum up to 107 GPa.

II. EXPERIMENTAL METHODS

A. Sample loading

For each high-pressure run, we use a five-step procedure to prepare a sample of platinum connected to two, three, or four electrical leads and thermally insulated from the diamond anvils by a layer of KCl. The result is an internally heated diamond anvil cell similar to the one used in Zha *et al.* [33] to measure the equation of state of platinum up to 80 GPa and

1900 K. Details are presented in the Supplemental Material [34]. Briefly, we first use standard methods to align diamond anvils with 100 to 300 μm-diameter culets and to make a preindented rhenium gasket with an insert made of cubic boron nitride mixed with ND 353 Epotek epoxy (hereafter referred to as "cBN"). Second, we prepare four outer electrodes that extend from the edge of body of the diamond cell to the edge of the diamond's culet. Third, we prepare the inner electrodes by pressing ~10 μm-thick pieces of platinum into the cBN on the culet.

Fourth, we laser drill a hole with diameter equal to 40% of the culet's diameter and fill it with several pieces of KCl and platinum. The pieces of platinum and KCl are stacked so that when the diamond cell is closed, one central piece of platinum of 5–30 μm-width is separated from both anvils by 5–10 μm-thick KCl layers and electrically connected to the four outer electrodes by other pieces of platinum. This central piece is the platinum sample that is eventually melted. Fifth, we dry the KCl by inserting the whole diamond cell in a vacuum oven for at least 45 min at 120 °C followed by an argon purge. Finally, we close the cell, let it cool, and compress to the target starting pressure. Pressure at room temperature is measured using the shift of the Raman signal from the strained diamond anvil [35]. After heating, pressure is measured again using the Raman edge or by x-ray diffraction from the 300 K platinum sample [36]. For each melting run, the reported pressure at room temperature, P_0, is the average of pressures measured before and after heating.

A simpler version of the above procedure was used for the sample that generated the lowest pressure data presented here. A diamond anvil cell was prepared with 1 mm-diameter culets, without a gasket, and with ~100 μm-thick KCl thermal insulation. The relatively large sample was made from a 0.5 mm-long segment of 25 μm-diameter platinum wire. Strips of gold were cut from 10 μm-thick foil and used as inner electrodes. The pressure before heating was less than 0.1 GPa.

B. Pulsed heating and electrical measurement

After compressing each platinum sample to high pressure, we connect it to the home-built electronics that drive current through the sample and measure current and voltage. First, each diamond cell is connected to the electronics, as shown in Fig. 1; see Supplemental Material [34] for details. Second, the capacitor bank is repeatedly discharged by delivery of square waves of 3 to 8 μs duration to the gate of the transistor (MOSFET). Third, the power of electrical heating pulses is gradually increased by increasing the voltage of the capacitor bank, V_{bank}, until the platinum sample reaches peak temperatures of 1500–2000 K, a temperature range that is high enough for a CCD camera to visualize the thermal emissions from the sample, yet low enough to avoid accidentally melting the sample. The current and voltage of each pulse (or set of pulses) is calculated based on an oscilloscope recording of the outputs of two instrumentation-amplifiers (in-amps). One in-amp measures the voltage difference across the reference resistor, while the other measures the voltage difference across the platinum sample.
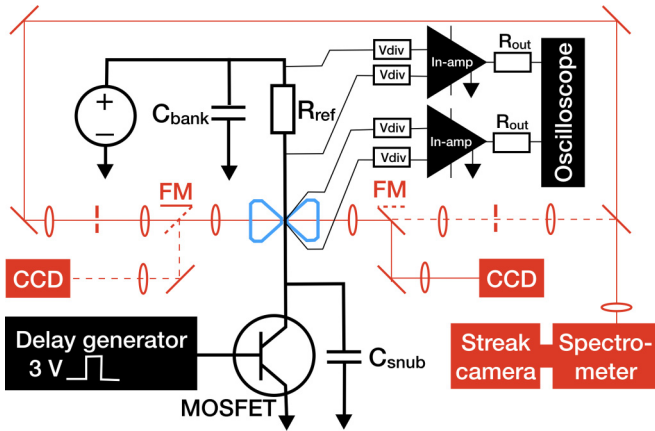
FIG. 1. Schematic of electrical path (black), optical paths (red), and diamond anvils (blue) at the Carnegie Institution for Science. A regulated dc power supply charges a capacitor bank (C_{bank}: 470 μF, 70 V electrolytic). When triggered by the Delay generator (SRS DG645), the MOSFET (FQP30N06L) allows current to flow through a reference resistor ($R_{ref} = 0.29$ Ω), and the platinum sample that is compressed between diamond anvils. The snubber capacitor (C_{snub}: 16 μF, 100 V electrolytic) limits current oscillations. The circuitry for measuring current and four-point-probe voltage are shown in thin black lines. The voltage dividers, Vdiv, reduce input voltage to within the 15 V range of the in-amp (AD842). Each divider is made of two resistors with typical values of 1 kΩ and 10 kΩ. The in-amp is operated with no gain, referenced to ground, and connected through output resistors (R_{out}: 105 Ω) to the oscilloscope (Tektronix DPO 3034). A simplified optical path is shown here; see McWilliams *et al.* [37] for elaboration. During each heating pulse, one flipper mirror (FM) diverts light from the left or right side of the diamond cell to a CCD camera (Point Grey Grasshopper3 Color) for two-dimensional imaging of thermal emissions. The other flipper mirror (FM) does not divert the light, allowing it to pass into a confocal filtering system, then into a spectrometer (Princeton Instruments Acton SP2300) and streak camera (Sydor ROSS 1000) for time-resolved measurements of thermal emissions. Solid red lines show the path of light in one configuration; dashed lines show the alternative configuration. Ovals represent lenses, line segments at 45° represent mirrors, and broken line segments represent pinholes.

C. Thermal emission and x-ray diffraction

While pulsing electrical power through the high-pressure sample, we measure time-resolved thermal emissions, spatially resolved thermal emission, and x-ray diffraction. Time-resolved measurements of thermal emissions are the key to detection of melting and freezing temperatures. Spatially resolved measurements of thermal emission are important for estimating the size of the sample that is melted. X-ray diffraction measurements are important for determining the crystallographic phase of the material that melts and its pressure evolution during heating.

We use two laboratories to generate the necessary data. The first melting experiment for each sample is performed at the Earth and Planets Laboratory of the Carnegie Institution for Science, where its thermal emissions spectra are recorded with a streak camera, a device that enables measurements with submicrosecond time resolution during single-heating-shot experiments. Several samples are subsequently melted

at GSECARS, Sector 13 of the Advanced Photon Source at Argonne National Lab. At GSECARS, atomic structure and temperature are monitored by x-ray diffraction and thermal emissions measurements on gated intensified detectors, not streak cameras. The detectors are gated to collect x-ray and optical photons when the sample reaches its highest temperature, the final 1 μs of the heating pulse.

In each laboratory, the sample is located at the focal position of the optical system. The Carnegie system is shown schematically in Fig. 1, and described in detail in McWilliams *et al.* [37]. The GSECARS system is described in Prakapenka *et al.* [38]. At GSECARS, the optical focus is aligned to the x-ray focus. V_{bank} is increased until the hottest section of the platinum sample is identified in an imaging camera set to 1 s exposure and maximum gain. Typically, we identify the hot spot by 10–100 repetitions of pulsed heating during the 1 s exposure. In all cases, a full cross section of the central platinum strip appears to heat to a nearly uniform temperature (Fig. S7). We then translate the sample so that the hot spot is at the focus of the optical system.

At Carnegie, we record thermal emissions on the streak camera (e.g., Fig. 2). The measurement's spectral range is 450–860 nm in all experiments but one; a higher-resolution grating limits the spectral range to 500–660 nm for the $P_0 = 31$ GPa data set. The streak camera is set to 3 or 10 μs sweep duration for all experiments except for melting the nongasketed sample ($P_0 = 1$ bar), for which sweep duration is 100 μs. We record thermal emissions from one side of the sample on the streak camera, and from the other side on a CCD camera. An example of thermal emissions data from one heating pulse to temperatures >5000 K at 68 GPa is shown in Fig. 2. Anomalies in thermal emission intensity during melting and freezing are easily identified in measurements of intensity versus time.

At GSECARS, temperatures are determined by fitting Planck functions to thermal emissions spectra emitted from a rectangular region of the sample that is 6 μm × 20 μm in area. This fit assumes gray-body emission [39]. The x-ray energy is 37 keV and its beam size is 3 × 4 μm. X-ray patterns are integrated using the DIOPTAS software [40]. The resistive heating pulse duration is 5–15 μs.

For each starting pressure, P_0, we collect data at a range of values of V_{bank}. Then, we change pressure and heat again, if desired. In practice, melting is only documented at different pressures for one sample, first during heating from $P_0 = 78$ GPa, then during heating from $P_0 = 60$ GPa.

III. RESULTS

We report measurements of thermal emissions, voltage, current, and x-ray diffraction of platinum compressed and heated to 107 GPa and ≈5000 K. We define a plateau region to be one in which a temperature proxy changes anomalously slowly in time, compared to rate of change before and after the plateaulike region. The primary temperature proxy used in this study is the fourth root of thermal emission intensity, $I^{1/4}$. (The fourth root is motivated by the Stephan-Boltzmann law, $I_{total} \propto T^4$.)

Our main results are (i) plateaulike regions in $I^{1/4}$ are reproducible and reversible upon cooling, (ii) electrical
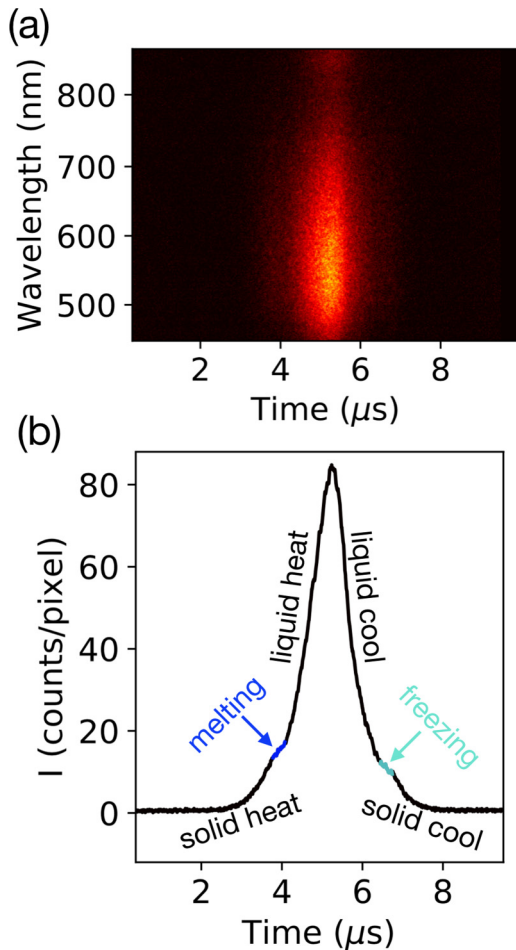
FIG. 2. Streak camera image of platinum heated from $T = 300$ K at $P = 60 \pm 3$ GPa to $T > 5000$ K. (a) Raw data. (b) Intensity averaged over the wavelength dimension. Annotations mark regions interpreted to be melting, freezing, and heating and cooling of solid and liquid platinum.

resistance measurements, calorimetric analysis, and x-ray diffraction show that the plateaulike regions are caused by latent heats of melting and freezing, and (iii) melting temperatures increase rapidly from 0 to ~40 GPa, then more gradually to 4490 ± 220 K at 107 ± 9 GPa (Fig. 5).

For each of 33 heating runs recorded on the streak camera, the melting region is identified as a plateaulike interval in $I^{1/4}$; six runs are shown in Fig. 3(b) and the remainder are shown in Figs. S8–S16. The melting temperature measured during an individual melting run is determined by fitting a Planck function to the thermal emissions spectrum collected during the melting interval (Fig. 3(d); Supplemental Material section "Temperature fits" [34]).

The pressure at melting is estimated by adding a heating-induced pressure to the room temperature pressure measurement, $P_m = P_0 + \Delta P$. The value of ΔP for each melting run is estimated from x-ray diffraction measurements at 30 to 60 GPa, assuming the equation of state of platinum determined by Matsui *et al.* [36]. Typically, $\Delta P = 8 \pm 4$ GPa (Supplemental Material section "Pressure at melting" [34]).

This process to determine the temperature and pressure of melting, T_m and P_m, yields highly reproducible results. Six melting runs are carried out at $P_m = 68 \pm 5$ GPa while measuring one side of the sample. These data are shown in Fig. 3; the other 27 melting runs are shown in Figs. S8–S16. For each side of each sample, plateaulike intervals occur at values of $I^{1/4}$ within 5% of each other and fitted temperatures are within 160 K (± 80 K) of each other (Table S1).

Including data collected from both sides of the sample (left-hand side and right-hand side), measured melting temperatures are more scattered (within ± 190 K for all but one sample; within ± 250 K for the sample measured with a narrow spectral range). All measured melting temperatures for each sample and starting pressure are averaged to determine T_m in a way that weights the two sides of the sample equally (Supplemental Material section "Temperature Fits at Melting" [34]). From sample to sample, the phenomenology of these measurements is reproducible, as shown in the figures of $dI^{1/4}/dt$ vs I (Figs. 3, S8–S16). The reproducibility can also be seen in the plots of dT/dt versus T described in Sec. IV.

Plateaulike regions are also documented upon cooling in 24 of the 33 heating runs in which a sample melted (Figs. 3, S8–S16). We interpret this as freezing. All freezing data show hysteresis; the value of $I^{1/4}$ in the plateaulike region is always slightly lower during cooling than during heating. The hysteresis could be caused by kinetics. The experimental timescale may be fast relative to growth kinetics for platinum crystallizing from a solid-melt interface, or relative to nucleation kinetics for platinum crystallizing at a platinum-KCl interface. The hysteresis could also result from increased temperature gradients during cooling, which cause the sample surface to be anomalously cold when the sample interior freezes and causes the plateaulike region.

The values of melting temperature increase monotonically within uncertainties, from 2170 K at low pressure (our non-gasketed sample) to 4540 K at 107 GPa [Fig. 4(a), Table I]. The slope, dT_m/dP, decreases two-fold from $\approx$40 K/GPa at ambient pressure to $\approx$20 K/GPa at 50–100 GPa, but no discontinuities in slope are identified. A fit to the Simon functional form, $T_m = T_0(P/A + 1)^{1/C}$, yields $A = 15.1$ and $C = 2.60$, assuming the ambient pressure melting temperature, $T_0 = 2041$ K. Our measurements of T_m deviate by up to 300 K from the Simon fit, so we summarize them by an error envelope of ± 300 K around the Simon fit (red shading in Fig. 5).

Before describing further experimental results, we summarize the key evidence for our melting interpretation based on the thermal emissions data alone: plateaulike regions are reproducible and reversible, and their temperatures increase monotonically with pressure. Moreover, extrapolation of our measurements to ambient pressure agrees with the known value of melting temperature, 2041 K, to within our measurement uncertainty (Fig. 5).

Further evidence that melting and freezing cause the plateaulike regions is provided by combined analysis of thermal emissions measurements with electrical and x-ray measurements. First, electrical resistance typically increases rapidly as a function of temperature during the plateaulike interval, as expected upon melting for a metal (Supplemental
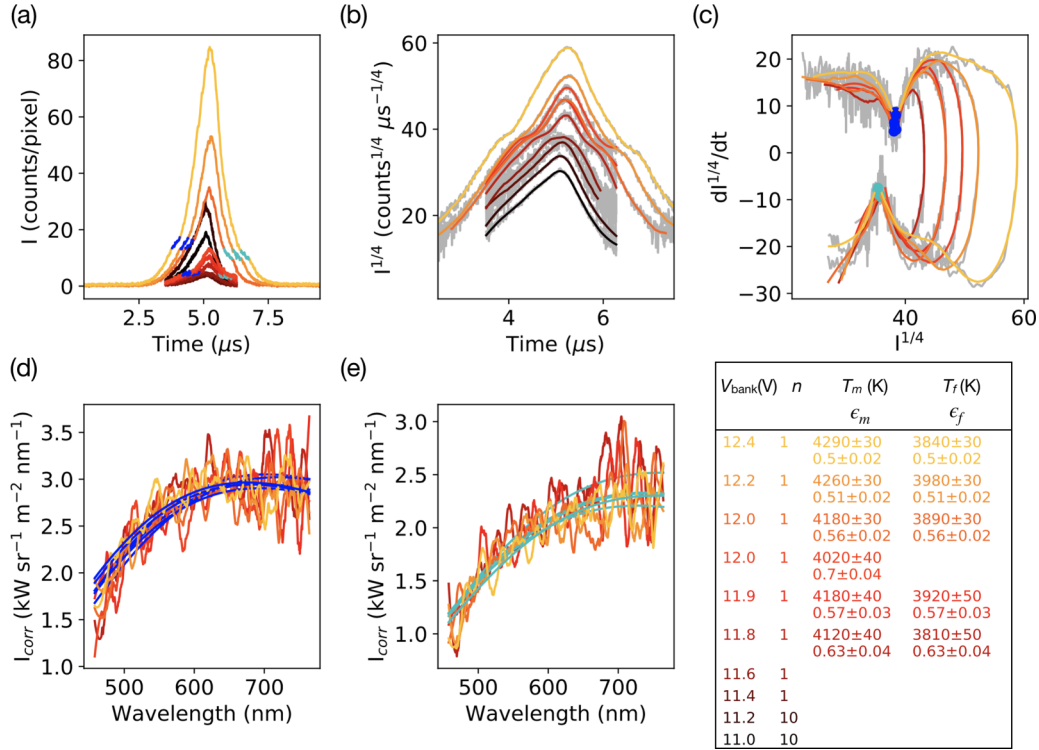
V_{bank}(V)	n	T_m (K)	T_f (K)
		ϵ_m	ϵ_f
12.4	1	4290±30	3840±30
		0.5±0.02	0.5±0.02
12.2	1	4260±30	3980±30
		0.51±0.02	0.51±0.02
12.0	1	4180±30	3890±30
		0.56±0.02	0.56±0.02
12.0	1	4020±40	
		0.7±0.04	
11.9	1	4180±40	3920±50
		0.57±0.03	0.57±0.03
11.8	1	4120±40	3810±50
		0.63±0.04	0.63±0.04
11.6	1		
11.4	1		
11.2	10		
11.0	10		

FIG. 3. Time-resolved thermal emissions of the left side of the platinum sample heated from 300 K at 60 ± 3 GPa to past its melting point at 4060 ± 140 K at 68 ± 5 GPa. Each warm color (yellow to red to black) represents a set of n heating pulses driven by the voltage that is listed in the legend (V_{bank}). Blue and cyan markings indicate melting and freezing. (a) Average counts on the streak camera CCD. (b) Fourth root of average counts per microsecond, a proxy for temperature. Noisy gray curves show unsmoothed data, $I^{1/4}$, while colored curves show smoothed data, $I_s^{1/4}$. (c) Time-derivatives, $\frac{dI_s^{1/4}}{dt}$ (grey), and smoothed time derivatives, $\frac{dI_s^{1/4}}{dt}_s$ (colors). The smoothing function is a second-order Savitzky-Golay filter with timescale $\tau = 0.4$ μs for both $I_s^{1/4}$ and $\frac{dI_s^{1/4}}{dt}_s$. The minima during heating (blue circles) and maxima during cooling (cyan circles), are interpreted as melting and freezing. The corresponding times, $t_{melt} \pm \tau/2$ and $t_{freeze} \pm \tau/2$, are marked in blue and cyan in (a), and used for the temperature fits in (d) and (e). (d), (e) Planck fits (blue and cyan) to thermal emissions spectra during melting and freezing. Planck fit parameters listed in the legend are melting temperature and emissivity (T_m and ϵ_m), and freezing temperature and emissivity (T_f and ϵ_f). Spectra have been filtered to improve the clarity of the figures using a second-order Savitzky-Golay filter with wavelength scale $d\lambda = 20$ nm. Planck fits are performed without filtering the spectra.

Material "Electrical resistance across melting"; Table S2 [34]).

Second, x-ray diffraction measurements show diminishing intensity of face centered cubic peaks and an increasingly intense diffuse background at temperatures near T_m (Figs. S5, S6). This rules out the possibility that the latent heat of a crystal-to-crystal phase transition is responsible for the plateaulike regions, at least at the pressures where diffraction was measured near melting (35–60 GPa). The x-ray measurements are not used to quantify melting temperature in this study. For details, see Sec. IV, the Supplemental Material section "X-ray diffraction near melting", and Figs. S5, S6 [34].

Third, the amount of electrical energy deposited during the plateaulike interval is similar to the anticipated value of latent heat plus heat lost to the surroundings. In the Supplemental Material section "Latent heat of melting" [34], we present a quantitative analysis of upper bounds on latent heat, L_{max}, and entropy change across melting, $\Delta S_{max} = L_{max}/T_m$. Briefly, we divide the excess Joule heating energy required to overcome the plateaulike region, E, by the volume of sample that melts, V, times the molar density of crystalline Pt at the melting pressure and temperature, ρ_m. Together, $L_{max} = E/V \rho_m$. Two uncertainties combine to make this a conservative upper bound on L: (i) the quantity E is only partially corrected for heat loss to the surroundings, and (ii) we propagate uncertainty in the measurement of V by subtracting the uncertainty dV in order to ensure L_{max} is an upper bound. Next, we divide by T_m to calculate an upper bound to the entropy of fusion, ΔS_{max}. At $P_m = 34$, 68, and 86 GPa, $\Delta S_{max} = 22$–37 J/mol/K, which is merely 2–3 times the ambient pressure value. This means that a modest entropy change is sufficient to explain plateaulike anomalies.

IV. DISCUSSION

A. Melting curve of platinum

The melting temperature of platinum increases from 2041 K at ambient pressure to 3300 K at 40 GPa, in line with the steep slopes documented in Refs. [3,12,14,41] (Fig. 5). Above 50 GPa, however, the slope is much shallower than reported by Anzellini et al. [12] and Belonoshko and Rosengren [3]. We find $dT_m/dP < 25$ K/GPa at all pressures from
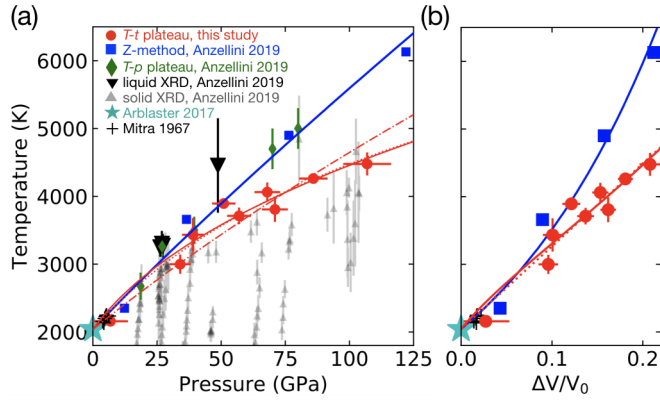
FIG. 4. Melting temperature of platinum as a function of (a) pressure and (b) compression. Experimental data from this study (red circles) are compared to experimental and computational data from Anzellini *et al.* [12], Mitra *et al.* [41], and Arblaster *et al.* [44]. X-ray diffraction-based identification of solid platinum and of liquid platinum from Anzellini *et al.* (small gray triangles and large black triangles, respectively) are consistent with our melting data, within the uncertainties. Observations of plateaus in temperature versus laser power (green diamonds) and calculations by the Z method (blue squares) from Anzellini *et al.* are consistent with our melting temperatures at pressures up to 40 GPa, but inconsistent at pressures above 60 GPa. Solid curves are Simon fits to the data of this study (red) and to the Z-method calculations of Anzellini *et al.* (blue). Kraut-Kennedy and Lindemann fits to the data of this study are shown by dotted red and dash-dotted red curves, respectively.

50–110 GPa. This decreasing slope is expected according to the Kraut-Kennedy empirical model, which predicts that T_m depends linearly on volume, not pressure [1]. Indeed, the volume dependence of latent-heat-based measurements of T_m clearly approximates a line that includes the ambient pressure melting point, $T_0 = 2041$ K [Fig. 4(b)]. The Z-method calculations could also be fitted to a line that includes ambient pressure melting, but the deviation would be $\approx$400–500 K at 12 GPa and 122 GPa. It is possible that calculations using the Z method with waiting time analysis would generate lower values of melting temperature [22,23].

Both the Lindemann and Kraut-Kennedy functions can be used to fit our melting data with one free parameter, and the Kraut-Kennedy fit has a lower root mean-square deviation. Note that the Lindemann model is sometimes used with zero free parameters, using known or assumed values of the

TABLE I. Melting points.

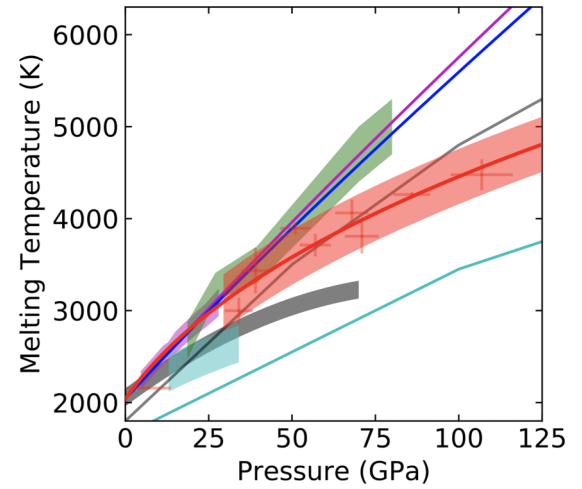| P_m (GPa)	T_m (K)
6.8 ± 6.8	2160 ± 20
34 ± 4.2	3000 ± 140
39 ± 4.3	3430 ± 250
51 ± 4.5	3890 ± 70
57 ± 4.7	3710 ± 120
68 ± 5	4060 ± 140
71 ± 5.1	3810 ± 190
85.9 ± 5.6	4260 ± 30
106.9 ± 9.3	4480 ± 170

FIG. 5. High-pressure melting curve of platinum. Melting data of this study (red crosses), the Simon fit to the data (solid red), and an error envelope of $\pm$300 K at pressures above 30 GPa (red shading). Past experimental studies are summarized by error envelopes: Anzellini *et al.* [12] (green), Errandonea [14] (magenta), Kavner and Jeanloz [15] (gray), Patel and Sunder [16] (cyan). Theoretical results are shown in solid curves: Belonoshko and Rosengren [3] (magenta), Anzellini *et al.* [12] (blue), Jeong and Chang [53] (gray), and Liu *et al.* [54] (cyan).

Gruneisen parameter, γ_0, and its pressure dependence, q, as well as an assumed value for the Lindemann parameter. Here, we use the formulation of the Lindemann model in Anderson and Isaak [42], in which the melting temperature at ambient pressure is fixed to its known value. We fix the value of γ_0 to 2.7 and allow q to be a fitting parameter, motivated by the fact that three experimental studies find similar values of γ_0 but very different values of q. Matsui *et al.* [36], Fei *et al.* [43], and Zha *et al.* [33] find $(\gamma_0, q) = (2.70, 1.1), (2.72, 0.5)$, and $(2.75, 0.25$ to $0.01)$, respectively. The Lindemann model is [42],

$$T_m = T_0 \left(\frac{V}{V_0}\right)^{2/3} \exp\left(\frac{2\gamma_0}{q}[1 - (V/V_0)^q]\right). \quad (1)$$

The Kraut-Kennedy model [1] has one free parameter, C.

$$T_m = T_0[1 + C(1 - V/V_0)]. \quad (2)$$

Here, V is volume, V_0 is the volume at ambient pressure. In both cases, we assume $T_0 = 2041$ K [44], and the room-temperature equation of state determined by Matsui *et al.* [36]. Note that here V refers to values along the melting curve, as in Refs. [2,42], unlike in Ref. [1]. The best fit parameter is $q = 1.04$ for the Lindemann model and $C = 6.0$ for the Kraut-Kennedy model (Fig. 5). Note that the value $q = 1.04$ is very close to 1.10, the value found in the equation of state study of Matsui *et al.* [36]. Nevertheless, the root mean-square deviation of Kraut-Kennedy fit to data is smaller than that of the Lindemann fit (190 K compared to 270 K), so we prefer the Kraut-Kennedy fit. Conveniently, the Kraut-Kennedy and Simon fits are nearly identical over the pressure range 0–120 GPa (Fig. 4). We highlight the Kraut-Kennedy fit in this paper rather than the Simon fit because it uses one free parameter rather than two.

Despite the agreement of our data to the melting curves of Refs. [3,12,14,41] at pressures below 40 GPa, our melting data are discrepant with previous experimental and computational results in several ways (Figs. 4–5). In the pressure range 40–80 GPa, the range of slopes of our melting curve, 25–18 K/GPa, is inconsistent with the 40 K/GPa slope reported in Anzellini *et al.* [12]. We associate the discrepancy to a difference in melt detection method. The only experimental constraint with <1000 K uncertainty for the melting curve of Anzellini *et al.* at pressures above 40 GPa is the saturation in temperature as the power of a continuous-wave laser is steadily increased, a phenomenon that is not specific to melting. Rather, it can be caused by surface reflectivity changes or movement of solid or liquid material [24]. In the pressure range 50–80 GPa, our melting temperatures are 300–1500 K higher than those reported in Lo Nigro [17] and in Kavner and Jeanloz [15], in which melting was determined by x-ray diffraction and visual observation, respectively. In the pressure range 80–120 GPa, our melting temperatures are 600–1000 K lower than those calculated by the Z method [3,12].

Our melting curve is consistent the x-ray diffraction data of Anzellini *et al.* [12] [Fig. 4(a)], and with our own x-ray diffraction data (Supplemental Material section "X-ray diffraction near melting" [34]), albeit within $\approx$1000 K uncertainties in determination of T_m from most of the x-ray diffraction measurements. At 30 GPa, Anzellini *et al.* reports a narrowly constrained melting temperature based on x-ray diffraction, and it agrees with the latent heat melting temperatures documented here (Fig. 4). At 50 GPa, Anzellini *et al.* reports the transition from solid to liquid diffraction in the range 3040–5130 K, the low-temperature end of the error bar for solid diffraction to the high-temperature end of the error bar for liquid diffraction. This $\pm$1000 K range spans our latent-heat melting data at 50 ± 10 GPa [Fig. 4(a)]. At 60–100 GPa, Anzellini *et al.* reports solid x-ray diffraction only, with error bars that overlap our melting data in all cases. The x-ray diffraction data from the present study are described in detail in Supplemental Material section "X-ray diffraction near melting" [34]. Briefly, we measure temperature and x-ray diffraction during the pulsed electrical heating of four samples during five heating runs to peak temperatures above the quantity ($T_m - 1000$ K), where T_m is the melting temperature based on our latent heat criterion. One heating run shows no kink in the plot of diffuse scattering intensity versus temperature [Fig. S5(o)], while the other four all show kinks within $\pm$1000 K of T_m [Figs. S5(c), S5(f), S5(i), S5(l)]. Only two of the runs showed kinks within $\pm$300 K of the latent heat melting temperature [Figs. S5(c), S5(f)]. In summary, there is agreement to within $\pm$1000 K between the latent heat melting temperatures and the x-ray diffraction data from this study and from Anzellini *et al.* [12]. To reduce the uncertainty in x-ray determination of melting, it may be important to invent new ways to contain a molten sample at pressures above 40 GPa and temperatures above 3000 K for longer times, and/or to use more intense x-ray sources.

B. Reproducibility of electrical heating and latent heat detection

The shape of the latent heat anomaly in $I^{1/4}$ versus t is reproducible at all pressures from 6.8 ± 6.8 GPa to
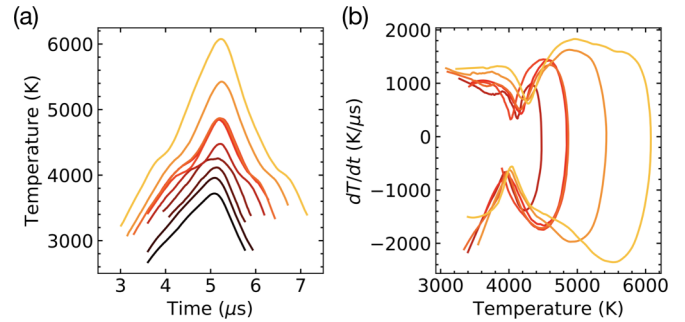

FIG. 6. Temperature evolution of platinum heated from room temperature at 60 ± 3 GPa during the same nine sets of heating runs shown in Fig. 3. Emissivity is fitted to emissions spectra from a narrow region of each curve. (a) Temperature, T, versus time, t. (b) Heating and cooling rates, dT/dt, versus T.

106.9 ± 9.3 GPa. Figures 3 and S8–S16 show 33 plateaulike regions in which the quantity $dI^{1/4}/dt$ consistently decreases temporarily before increasing again. But rather than rely on ten figures to document the reproducibility of the new melt-identification method, we can further process the data and generate a single, easy-to-read figure.

We convert intensity, I, to temperature, T, using a two-step process that assumes constant emissivity during each heating run. First, we use spectroradiometry, as in the determination of T_m described above. Planck functions are fit to thermal emissions spectra averaged over a single time interval, using two free parameters, temperature, and emissivity. The time interval is the plateaulike melting interval if exists, and the most intense $\approx$1 μs otherwise. Second, fixing the fitted value of emissivity, ϵ, we use pyrometry to determine temperature. We numerically solve for the following equation for temperature, T, at each time, t:

$$\int_{\lambda_1}^{\lambda_2} \epsilon \times \text{Planck}(T, \lambda) d\lambda = \int_{\lambda_1}^{\lambda_2} I_{\text{sam}}(\lambda, t) d\lambda. \quad (3)$$

Here, "Planck" is the Planck function for black-body radiation, $\lambda_1 = 450$ nm, and $\lambda_2 = 860$ nm for all data sets except the data set with $P_m = 39$ GPa, for which $\lambda_1 = 500$ and $\lambda_2 = 660$ nm. The measured intensity, I_{sam}, is corrected for optics and camera efficiency by the usual calibration with a standard tungsten lamp.

The temperature evolution is shown in Fig. 6(a) for nine heating runs starting at $P_0 = 60$ GPa. The temperature-time function has been filtered through to a second-order Savitzky-Golay filter with the same timescale, τ used in plots of $I^{1/4}$ vs t. Then temperature is differentiated with respect to time, and a second, identical Savitzky-Golay filter is used to reduce the noise in dT/dt. The resulting values of dT/dt versus T are plotted in Fig. 6(b) for the melting data at $P_0 = 60$ GPa ($P_m = 68$ GPa), and truncated to show only the melting region in Fig. 7 for all 33 melting runs at $P_m = 7$–107 GPa.

Figure 7 shows the signature of melting in all data used to generate the melting curve of platinum to 107 GPa. Latent heat absorption manifests as clear dips in the plots of dT/dt versus T. Moreover, the dips in dT/dt are transient in all cases; temperature increases again after latent heat is absorbed. The variation in temperature of dT/dt minima in
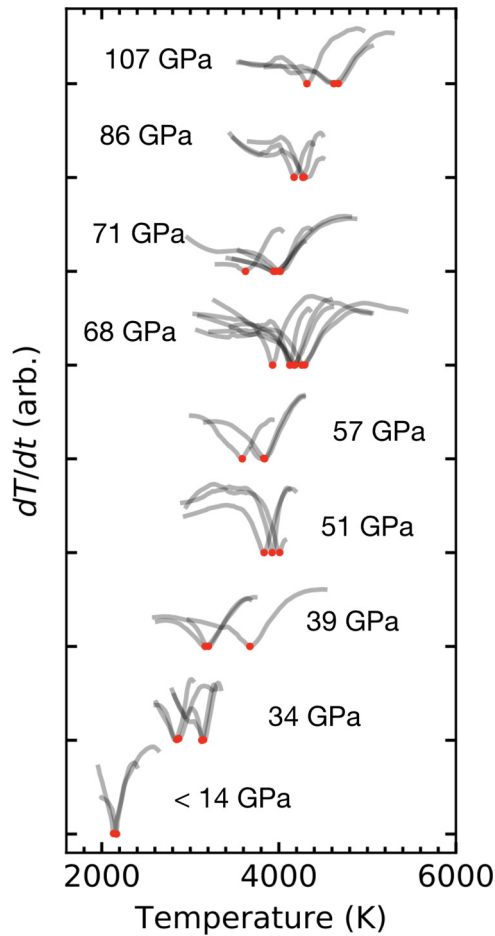
FIG. 7. Signature of latent heat absorption during all melting runs documented in this study. The rate of temperature change, dT/dt, is plotted against temperature, T (gray curves). The dip in each curve is caused by the latent heat of melting. Values of dT/dt are scaled and offset so that each cluster of curves reflects all the melting data generated by heating from a single starting pressure.

FIG. 8. Temperature evolution of platinum heated from room temperature at 60 ± 3 GPa, assuming a fixed emissivity of 0.58. The data are from the same nine sets of heating runs shown in Figs. 3, 6. (a) Temperature, T, versus time, t. (b) Heating and cooling rates, dT/dt, versus T.

[8,11,45–51]. Second, some studies show that the shape of the temperature-laser power anomaly is not reproducible, with sample temperature increasing after a plateau during some heating runs and decreasing after a plateau in other heating runs [46]. This variability can be caused by changes in the sample surface, which causes changes in the efficiency of laser absorption [24]. Whereas the properties of a metal's surface can change at temperatures below or above the melting temperatures and can result in more or less absorption, the latent heat of melting is only absorbed upon melting and only released upon freezing. This may crucial be to the reproducibility of the plateaulike anomalies in the data presented here.

The relatively high reproducibility of heating platinum to a liquid state may be useful for future studies, since containing a liquid in a diamond cell is a major technical challenge. In some cases, pulsed resistively heated samples can be repeatedly heated to well above their melting points. The two most outstanding heating runs were performed on one sample at $P_0 = 43$ GPa, and one sample at $P_0 = 60$ and 78 GPa. The former was melted several hundred times while monitoring x-ray diffraction and electrical resistance. The latter was reproducibly melted nine times, reaching more than 1000 K above the melting temperature during one pulse. In both cases, the stress state inside the gasket hole was relatively isotropic, as evidenced by the lack of increasing hole diameter upon compression at room temperature prior to the melting experiment. By contrast, in cases where the gasket hole visibly expanded during compression, which suggests significant axial stress, the melted segment of the sample seemed to narrow. This narrowing caused the peak temperature to increase when repeatedly heating with a constant driving voltage, V_{bank}.

For several samples, resistivity increases during melting provide a second indication of melting, and can be identified at every melting repetition using an oscilloscope. This melt identification technique could be used in an automated feedback loop to reproducibly heat a sample to slightly above its melting temperature. In fact, a manual feedback loop was employed during some of the x-ray diffraction measurements. We manually adjusted V_{bank} during sequences of 1000 melting shots so that the onset of melting, as observed by a kink in

Figs. 6 and 7 seems to be caused by the uncertainty in Planck fits. If instead of using a two-parameter Planck fit, we fix the value of emissivity for several streak camera images collected from one side of one sample, we find much less variation. An example is shown in Fig. 8. By fixing emissivity to the 0.58, the mean of emissivities fitted using two-parameter Planck fits, dT/dt minima range from 4140–4180 K, which is seven times less variation than the range of dT/dt minima found when emissivity is allowed to vary from image to image (4020–4290 K). In other words, the precision of our measurement of plateaus in $I^{1/4}$ propagates to ± 20 K uncertainty in temperature, but the precision of the temperature measurement itself is only ± 140 K since it combines uncertainties in $I^{1/4}$ and emissivity. The reproducibility of measurement of plateau temperature from side to side and sample to sample is ± 300, suggesting this is the accuracy of the melting curve.

The latent heat plateaus documented in this study are different than plateaus documented in studies that use continuous laser heating. First, the observation interpreted as a melting plateau in temperature versus laser power rarely show temperatures increasing again after the plateau region
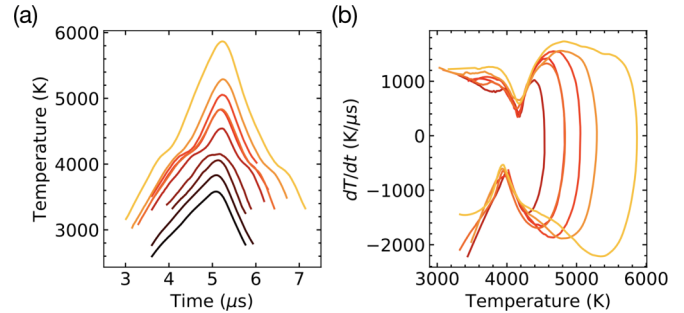
four-point probe voltage, occurred $\approx 2~\mu$s before the end of the heating pulse.

C. Latent heat versus other sources of anomalous temperature change

This is likely the first time that latent heats have been detected in static compression experiments at pressures >20 GPa, despite several claims of latent heat detection in diamond cells. Most previous studies have suffered from slow heating timescales ($\gg \mu$s for diamond-cell-sized samples), which causes thermal conduction out of the sample to dominate the temperature evolution.

Five alternative explanations for the plateaulike regions are possible, but unlikely. First, the plateaulike regions could be caused by a solid-solid phase transition to a high-temperature solid with entropy nearly as high as that of liquid platinum. In this scenario, the latent heat of melting would be dwarfed by the latent heat of the solid-solid transition, obscuring the melting plateau while highlighting the solid-solid plateau. Two pieces of evidence make this unlikely. First, such a solid is not predicted for platinum at high pressure, and not observed for any elemental metal at ambient pressure. Even solid Fe and Ti, whose entropies increase substantially upon solid-solid transitions above 1000 K, still maintain entropies that are significantly smaller than their liquids [26]. Second, the x-ray diffraction data at 35–55 GPa reveal no crystalline peaks besides fcc platinum, even when the temperature of the heated region of the sample exceeds the temperature of the plateaulike region.

A second alternative explanation is that the latent heat of fusion of KCl causes the plateaulike regions. This scenario would require very large values for thermal conductivity of KCl so that the sample's surface temperature evolution is significantly affected by heat absorption in KCl. In reality, we expect the sample's surface temperature to be much more strongly affected by the highly conductive platinum than the low thermal conductivity KCl in part because of the contrast in thermal conductivities and in part because Joule heat is deposited in the platinum only. Still, thermal modeling would be required to quantify possible effects of the latent heat of KCl on the temperature evolution of the platinum surface.

Third, an approximately tenfold increase in thermal conductivity of the KCl medium would decrease the slope of temperature versus time, as modeled in Fig. 7 of Geballe and Jeanloz [24]. However, the decrease would be maintained at all temperatures above the transition temperature. To reproduce the plateaulike observations, a sequence of transitions would be required in which the thermal conductivity of KCl increased approximately tenfold and then decreased approximately tenfold. This sequence would be unprecedented for an alkali halide at any pressure, to the best of our knowledge.

A fourth alternative explanation is that platinum transitions to a low resistivity phase at high temperature, causing a plateau in Joule heating power. This would lead to a plateaulike region in the same way that reflectivity increases have been shown to cause plateaulike regions in models of pulsed laser heating [24,31,32]. However, we infer the opposite from our electrical data: resistance increases with temperature by 3–10% in the plateaulike region for several

of the samples (Table S2), and no decrease in resistance with increasing temperature is detected for any sample.

A fifth possibility is that a near-melting phenomenon, such as fast recrystallization, surface premelting, or bulk premelting, causes the plateaulike regions. Fast recrystallization of several metals has been detected at temperatures that are hundreds of K below melting in diamond cells, using sequences of $\approx$1 s x-ray diffraction images (e.g., Refs. [10,11,52]). However, recrystallization at the $\approx$ 1 s timescale would not affect our microsecond-timescale melting experiments. Premelting would introduce anomalously high specific heat at temperatures below melting, biasing the temperature measurement of the plateaulike region to lower values. However, we do not know of any prediction of bulk premelting for platinum. If premelting were restricted to surface (i.e., less than a few nanometers), we would expect a very small downward shift in the temperature of the plateaulike region since the heat capacity of the sample's interior has a much larger effect than the surface heat capacity on temperature evolution at our heating timescale; a 1 μs timescale yields a thermal diffusion length scale of $\sqrt{D\tau} = 7~\mu$m at $\approx$50 GPa and 2000 K, assuming thermal conductivity from McWilliams *et al.* [37], the equation of state from Matsui *et al.* [36], and a heat capacity of three times the gas constant.

V. CONCLUSIONS

Using microsecond-timescale pulsed electrical heating in diamond anvil cells, detection of melting and freezing by latent heat is reproducible and reversible. Plateaulike regions in thermal emission intensity versus time are reproducible to $\pm 5\%$ intensity, which is equivalent to ± 20 K. Planck fits to determine temperature are reproducible to ± 140 K. Reproducibility is ± 190 K among all melting runs for both surfaces of each sample, excluding the one sample measured with a narrow spectral range. Moreover, the shape of plateaulike anomalies in $I^{1/4}$ versus time is reproducible for both surfaces of all samples at all pressures. These successes suggest that the new technique is an excellent candidate for further studies of melting and freezing experiments on a wide range of metals at megabar pressures and temperatures to at least 5000 K.

The melting curve of platinum measured by the latent heat method is steeply sloped from ambient pressure to $\approx$40 GPa. At higher pressure the slope, dT_m/dP, decreases smoothly to $\approx$15 K/GPa at 100 GPa, departing from the results of *ab initio* Z-method calculations published so far. As a function of compression, on the other hand, melting temperature increases linearly over the 0–20 % range of compression studied here, allowing a good fit to the Kraut-Kennedy empirical model with fit parameter $C = 6.0$.

[1] E. A. Kraut and G. C. Kennedy, Phys. Rev. Lett. **16**, 608 (1966).

[2] J. J. Gilvarry, Phys. Rev. **102**, 308 (1956).

[3] A. B. Belonoshko and A. Rosengren, Phys. Rev. B **85**, 174104 (2012).

[4] K. Hirose, S. Labrosse, and J. Hernlund, Ann. Rev. Earth Planet. Sci. **41**, 657 (2013).

[5] E. A. Kraut and G. C. Kennedy, Phys. Rev. **151**, 668 (1966).

[6] D. Errandonea, S. G. MacLeod, L. Burakovsky, D. Santamaria-Perez, J. E. Proctor, H. Cynn, and M. Mezouar, Phys. Rev. B **100**, 094111 (2019).

[7] D. Errandonea, L. Burakovsky, D. L. Preston, S. G. MacLeod, D. Santamara-Perez, S. Chen, H. Cynn, S. I. Simak, M. I. McMahon, J. E. Proctor, and M. Mezouar, Commun. Mater. **1**, 60 (2020).

[8] R. Sinmyo, K. Hirose, and Y. Ohishi, Earth Planet. Sci. Lett. **510**, 45 (2019).

[9] R. Hrubiak, Y. Meng, and G. Shen, Nature Commun. **8**, 14562 (2017).

[10] V. Stutzmann, A. Dewaele, J. Bouchet, F. Bottin, and M. Mezouar, Phys. Rev. B **92**, 224110 (2015).

[11] P. Parisiades, F. Cova, and G. Garbarino, Phys. Rev. B **100**, 054102 (2019).

[12] S. Anzellini, V. Monteseguro, E. Bandiello, A. Dewaele, L. Burakovsky, and D. Errandonea, Sci. Rep. **9**, 13034 (2019).

[13] A. Karandikar and R. Boehler, Phys. Rev. B **93**, 054107 (2016).

[14] D. Errandonea, Phys. Rev. B **87**, 054108 (2013).

[15] A. Kavner and R. Jeanloz, J. Appl. Phys. **83**, 7553 (1998).

[16] N. N. Patel and M. Sunder, in *DAE Solid State Physics Symposium 2017*, AIP Conf. Proc. No. 1942 (AIP, Melville, NY, 2018), p. 030007.

[17] G. Lo Nigro, Ph.D. thesis, Université Blaise Pascal-Clermont-Ferrand II, 2011.

[18] A. Lazicki, Y. Fei, and R. J. Hemley, Solid State Commun. **150**, 625 (2010).

[19] H. D. Luedemann and G. C. Kennedy, J. Geophys. Res. **73**, 2795 (1968).

[20] G. H. Wolf and R. Jeanloz, J. Geophys. Res. **89**, 7821 (1984).

[21] F. D. Stacey, S. S. Spiliopoulos, and M. A. Barton, Phys. Earth Planet. Inter. **55**, 201 (1989).

[22] D. Alfè, C. Cazorla, and M. J. Gillan, J. Chem. Phys. **135**, 024102 (2011).

[23] J. Braithwaite and L. Stixrude, Geophys. Res. Lett. **46**, 2037 (2019).

[24] Z. M. Geballe and R. Jeanloz, J. Appl. Phys. **111**, 123518-123518-15 (2012).

[25] A. Karandikar, Ph.D. thesis, Goethe-Universitat, Frankfurt am Main, 2006.

[26] R. Hultgren, L. Orr, P. D. Anderson, and K. K. Kelley, *Selected Values of Thermodynamic Properties of Metals and Alloys* (John Wiley and Sons, New York, 1963).

[27] C. Cagran and G. Pottlacher, in *Handbook of Thermal Analysis and Calorimetry - Recent Advances, Techniques, and Applications*, 5th ed., edited by M. E. Brown and P. K. Gallagher (Elsevier, Amsterdam, 2008), Vol. 5, Chap. 9, pp. 299–320.

[28] S. Deemyad and I. F. Silvera, Phys. Rev. Lett. **100**, 155701 (2008).

[29] M. Zaghoo, A. Salamat, and I. F. Silvera, Phys. Rev. B **93**, 155128 (2016).

[30] M. Houtput, J. Tempere, and I. F. Silvera, Phys. Rev. B **100**, 134106 (2019).

[31] J. A. Montoya and A. F. Goncharov, J. Appl. Phys. **111**, 112617 (2012).

[32] A. F. Goncharov and Z. M. Geballe, Phys. Rev. B **96**, 157101 (2017).

[33] C.-S. Zha, K. Mibe, W. A. Bassett, O. Tschauner, H.-K. Mao, and R. J. Hemley, J. Appl. Phys. **103**, 054908 (2008).

[34] See Supplemental Material at http://link.aps.org/supplemental/10.1103/PhysRevMaterials.5.033803 for further methodological details as well as detailed results from each melting run.

[35] Y. Akahama and H. Kawamura, J. Appl. Phys. **100**, 043516 (2006).

[36] M. Matsui, E. Ito, T. Katsura, D. Yamazaki, T. Yoshino, A. Yokoyama, and K.-i. Funakoshi, J. Appl. Phys. **105**, 013505 (2009).

[37] R. S. McWilliams, Z. Konôpková, and A. F. Goncharov, Phys. Earth Planet. Inter. **247**, 17 (2015).

[38] V. B. Prakapenka, A. Kubo, A. Kuznetsov, A. Laskin, O. Shkurikhin, P. Dera, M. L. Rivers, and S. R. Sutton, High Pressure Res. **28**, 225 (2008).

[39] L. R. Benedetti and P. Loubeyre, High Pressure Res. **24**, 423 (2004).

[40] C. Prescher and V. B. Prakapenka, High Pressure Res. **35**, 223 (2015).

[41] N. R. Mitra, D. L. Decker, and H. B. Vanfleet, Phys. Rev. **161**, 613 (1967).

[42] O. L. Anderson and D. G. Isaak, Am. Mineral. **85**, 376 (2000).

[43] Y. Fei, A. Ricolleau, M. Frank, K. Mibe, G. Shen, and V. Prakapenka, Proc. Nat. Acad. Sci. USA **104**, 9182 (2007).

[44] J. W. Arblaster, Johnson Matthey Tech. Rev. **62**, 80 (2017).

[45] G. Shen and P. Lazor, J. Geophys. Res. **100**, 17,699 (1995).

[46] O. T. Lord, M. J. Walter, R. Dasgupta, D. Walker, and S. M. Clark, Earth Planet. Sci. Lett. **284**, 157 (2009).

[47] O. T. Lord, M. J. Walter, D. P. Dobson, L. Armstrong, S. M. Clark, and A. Kleppe, J. Geophys. Res. (Solid Earth) **115**, B06208 (2010).

[48] O. T. Lord, I. G. Wood, D. P. Dobson, L. Vočadlo, W. Wang, A. R. Thomson, E. T. H. Wann, G. Morard, M. Mezouar, and M. J. Walter, Earth Planet. Sci. Lett. **408**, 226 (2014).

[49] A. Dewaele, M. Mezouar, N. Guignot, and P. Loubeyre, Phys. Rev. B **76**, 144106 (2007).

[50] A. Dewaele, M. Mezouar, N. Guignot, and P. Loubeyre, Phys. Rev. Lett. **104**, 255701 (2010).

[51] T. Kimura, H. Ohfuji, M. Nishi, and T. Irifune, Nature Commun. **8**, 15735 (2017).

[52] S. Anzellini, A. Dewaele, M. Mezouar, P. Loubeyre, and G. Morard, Science **340**, 464 (2013).

[53] J.-W. Jeong and K. J. Chang, J. Phys. Condens. Matt. **11**, 3799 (1999).

[54] Z.-L. Liu, J.-H. Yang, Z.-G. Zhao, L.-C. Cai, and F.-Q. Jing, Phys. Lett. A **374**, 1579 (2010).